

Power Dissipation in a Hard Superconducting Tube

C. R. WISCHMEYER

Rice University, Houston, Texas

(Received 25 July 1966)

Two kinds of dissipation are computed for a macroscopically homogeneous sample subjected to a changing axial magnetic field. Based upon the Anderson-Kim model of critical states, the induction, current density, electric field intensity, and thence the Joulean power density are determined. All are significantly dependent upon radial distance and magnetic history. Reversal of an applied field produces within the sample an interface region in which neighboring fluxoids are in opposite directions. Pairs of opposing fluxoids are presumed to coalesce, giving up their line energies as heat in an annihilation process. By way of illustration, computed values of all these quantities are presented for a typical unannealed $\text{Nb}_{0.75}\text{Zr}_{0.25}$ sample. If the computed values of dissipation, which are averages in the sense that they are based upon a homogeneous model, are taken to be a measure of the thermal activation of flux motion, then their pattern affords a highly satisfactory explanation of an extensive body of experimental observations.

I. INTRODUCTION

WHEN a thin-walled tube of hard superconductor is subjected to a changing axially applied magnetic field, flux creep and catastrophic flux jumps may be observed. Flux creep is characterized as a thermally activated process, and the initiation of flux jumps is attributed to local heating. It is therefore our object here to determine the power dissipation produced by the application of the field. The resulting Joulean heating is derived in terms of sample dimensions, material parameters, and rate of change of the applied field.

The Anderson-Kim model of critical states and tube magnetization is used to obtain, as a function of radius, expressions for magnetic induction and current density, and, in conjunction with Faraday's law, to obtain electric field intensity. Joulean power density is then found by multiplying current density by electric field intensity. As will become apparent, the power is significantly dependent upon radial distance as well as magnetic history and is proportional to rate of change of applied field.

The application of a large magnetic field and its subsequent reversal produce within the sample an interface region in which neighboring fluxoids are in opposite directions. Pairs oppositely directed are presumed to coalesce and give up their respective line energies as heat in an annihilation process. Where it occurs, this dissipation is also calculated.

The relationship of calculated values of power dissipation to experimental observations for various conditions of applied field are examined.

II. CRITICAL-STATE MODEL

The geometry of a thin-walled cylindrical tube was used earlier by Kim *et al.*¹ for reasons of experimental elegance. Not only does it permit direct measurement of a field quantity (on the tube axis) which reflects the tube magnetization of the superconductor, but also the

direct observation by means of pickup coils of the effects of flux creep² and flux jumps as induced voltage.

Here we exploit the tractability of this geometry in our analysis. We employ the model of critical states³ as defined by Kim *et al.*^{1,4} We consider the case in which the sample is maintained in a critical state by an axially applied field H , with dH/dt held constant. Since the lower critical field H_{c1} of the material of interest is so low compared to our applied fields, we shall assume the critical-state relations throughout.

The superconducting sample tube is assumed to be macroscopically homogeneous, that is, the material parameters⁴ α_c and B_0 and the temperature T are assumed uniform throughout the sample and constant. This assumption leads to *average* results in the sense that momentary effects of localized variations of flux motion⁵ are concealed.

The fact that the materials of interest here have relative permeability of unity has led to the more or less interchangeable use of B and H in much of the literature.

Critical-State H' - H Paths

Since the essence of the critical-state tube magnetization of Kim *et al.*^{1,4} is central to our problem, its relevant portions will be restated and inferences applicable to the present problem will be derived.

Let an axial field H be applied, which sets up a distribution of (circumferential) wall current density $J(r)$ and of induction $B(r)$. Inside the tube of wall thickness w the field is H' . Note that radial distance r is measured inward from the outside surface, while R is the corresponding radius. (See Fig. 1.)

Kim *et al.*⁴ have found essentially that the dependence of H' upon H in the case of a thin-walled circular tube may be represented by the hyperbolas

$$(H' + B_0)^2 - (H + B_0)^2 = \mp 0.8\pi\alpha_c w. \quad (1)$$

² P. W. Anderson, Phys. Rev. Letters **9**, 309 (1962).

³ C. P. Bean, Phys. Rev. Letters **8**, 250 (1962).

⁴ Y. B. Kim, C. F. Hempstead, and A. R. Strnad, Phys. Rev. **131**, 2486 (1963).

⁵ C. R. Wischmeyer, Phys. Letters **19**, 543 (1965).

¹ Y. B. Kim, C. F. Hempstead, and A. R. Strnad, Phys. Rev. Letters **9**, 306 (1962).

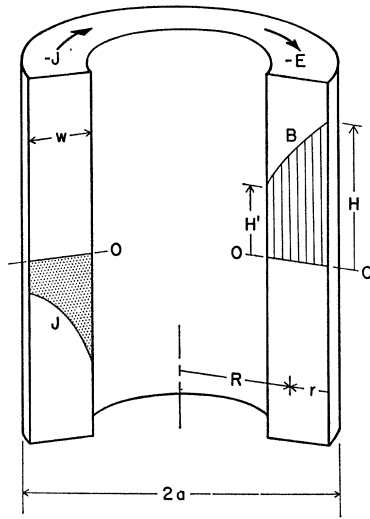


FIG. 1. Cutaway view of a hard superconducting tube in an increasing field (shielding region), showing directions of circumferential electric field E and current density J and the radial variation of J and induction B .

The minus sign accompanies increasing H (shielding region, with $H > H'$) and the plus sign decreasing H (trapping region, with $H < H'$). The existence of two curves implies irreversibility or hysteresis. α_c is essentially the largest gradient of magnetic pressure which the material will withstand; B_0 is a parameter descriptive of the sample. (See Fig. 2.)

It is relevant to recall that (1) describes a quasi-equilibrium state in which flux creep occurs in a negligible degree on a laboratory time scale. Also we observe that the behavior of tube magnetization described by (1) is independent of the means by which H is applied. For example, H applied to a tube might actually be the field inside a larger tube surrounding the first. This enables visualizing a tube of thickness w as the composite of a number of concentric laminae, in contact, of combined thickness w .

It is not unforeseeable that contained in the description of tube magnetization for increasing and for decreasing positive fields there is implicit a certain behavior upon reversal of the applied field. Upon reversal, the negative applied field opposes the positive trapped flux. An outer shell in a shielding regime (negative values of induction decreasing to zero with depth below the outside surface) surrounds an inner shell still in a trapping regime (induction increasing from zero, with depth, to the positive value H' of trapped field surrounded by the tube).

Suppose the interface between the two regimes, at which the local field passes through zero, is located at depth r_0 . To describe this negative shielding regime we modify (1):

$$(0 - B_0)^2 - (H - B_0)^2 = -0.8\pi\alpha_c r_0. \quad (2)$$

Similarly, to describe the positive trapping regime

$$(H' + B_0)^2 - (0 + B_0)^2 = 0.8\pi\alpha_c (w - r_0). \quad (3)$$

Subtracting (2) from (3), we obtain the description

of critical states for reversed H , which is implied by (1):

$$(H' + B_0)^2 + (H - B_0)^2 = 2B_0^2 + 0.8\pi\alpha_c w. \quad (4)$$

Understandably this is called the circular region, where H is negative and H' positive. (Again, see Fig. 2.)

Non-Critical-State Paths

Here we refer to circumstances in which less than the entire wall thickness w is in a critical state, which implies that no net flux creep across w is present.

Regardless of the initial field in which the sample is cooled, an initial point on the 45-degree line $H' = H$ is established. Consider first cooling in zero field, in which case the initial point is the origin. Subsequent application of H produces penetration of the bulk superconductor by the magnetic field from the outside inward as H exceeds H_{c1} . However, H' remains zero for $0 < H < H_s$, which we shall call the initial penetration range. At $H = H_s$, the flux front penetrates the wall thickness w ; and further increase of H will cause H' to rise from zero.

Cooling in a nonzero field likewise requires a subsequent change in H to generate circumferential currents and then to carry the sample into a critical state.

Another non-critical-state situation results whenever the applied dH/dt is reversed. The resulting path is again horizontal in the $H' - H$ plane, along which readjustment of the current density and local field occur.

III. COMPUTATION OF JOULEAN DISSIPATION

For the shielding and trapping regions variation of induction B and current density J across the wall thickness are readily obtained. To obtain $B(r)$ we simply replace H' by $B(r)$ and w by r in (1). Interpreting the double sign as before and solving, we have

$$B(r) = [(H + B_0)^2 \mp 0.8\pi\alpha_c r]^{1/2} - B_0. \quad (5)$$

Differentiating (5), the corresponding current density turns out to be

$$J(r) = \frac{1}{0.4\pi} \frac{dB(r)}{dr} = \mp \alpha_c [(H + B_0)^2 \mp 0.8\pi\alpha_c r]^{-1/2} \\ = \mp \alpha_c / [B(r) + B_0]. \quad (6)$$

For the circular region, similar expressions for induction and current density may be written, treating the layers in the negative shielding regime and the positive trapping regime separately. It is the outer layer (negative shielding regime) which sees the (negative) applied field H . We solve (2) for the radial thickness of this layer.

$$r_0 = H(H - 2B_0)(0.8\pi\alpha_c)^{-1}. \quad (7)$$

Hence, for $0 < r_s < r_0$, where r_s is radial depth measured inward,

$$B(r_s) = [(H - B_0)^2 - 0.8\pi\alpha_c r_s]^{1/2} - B_0 \quad (8)$$

and

$$J(r_S) = \alpha_c [(H - B_0)^2 - 0.8\pi\alpha_c r_S]^{-1/2}. \quad (9)$$

The inner layer (positive trapping regime), of radial thickness $(w - r_0)$, sees zero "external" field. Hence for $0 < r_T < (w - r_0)$, where r_T is radial depth measured inward from the interface at r_0 ,

$$B(r_T) = [B_0^2 + 0.8\pi\alpha_c r_T]^{1/2} - B_0 \quad (10)$$

and

$$J(r_T) = \alpha_c [B_0^2 + 0.8\pi\alpha_c r_T]^{-1/2}. \quad (11)$$

Hence, the combination of (8) and (10) and of (9) and (11) are required to describe induction and current density across the wall thickness.

The description of the initial penetration range is obtained from that of the shielding regime. Setting (5) equal to zero for the penetration depth $r = r_P$, we obtain

$$r_P = H(H + 2B_0)(0.8\pi\alpha_c)^{-1}. \quad (12)$$

For $0 < r < r_P$, (5) and (6) yield induction and current density.

Induced Electric Field

To obtain an expression for the electric field intensity E , we write Faraday's law in cylindrical coordinates. Since our applied magnetic field has only an axial component, the electric field has only a circumferential component. Hence

$$\nabla \times E = -\frac{1}{R} \frac{\partial(RE)}{\partial R} = -10^{-8} \frac{\partial B}{\partial t}, \quad (13)$$

where E is in V/cm and B in G. Rather than radial depth r , it is now more convenient to use the radius R cm. Integrating, we find the electric field at radius R_1 is

$$E(R_1) = -\frac{10^{-8}}{R_1} \int_0^{R_1} \frac{dB}{dt} R dR. \quad (14)$$

In the shielding region, the electric field in the superconducting material consists of contributions at-

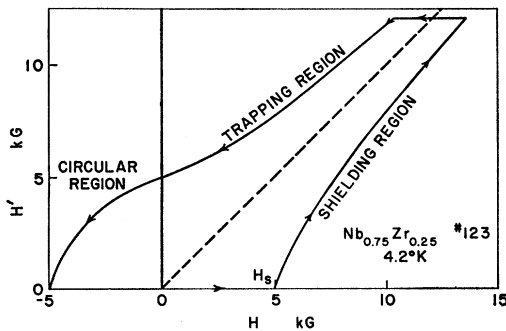


FIG. 2. Critical-state paths for unannealed $\text{Nb}_{0.75}\text{Zr}_{0.25}$ tube No. 123. Outside radius = 4 mm; wall thickness = 1.5 mm. $\alpha_c = 1.2 \times 10^8$ GA/cm²; $B_0 = 2.1$ kG.

tributable to changing induction in the volume surrounded by the tube and in the volume of the superconductor itself out to radius R_1 . That is,

$$E(R_1) = -\frac{10^{-8}}{R_1} \left[\int_0^{a-w} \frac{dH'}{dt} R dR + \int_{a-w}^{R_1} \frac{dB_S}{dt} R dR \right], \quad (15)$$

where H' is the field in the volume surrounded by the tube, given by (1), and B_S is the induction in the superconductor, obtained from (5), using the minus (upper) sign.

The corresponding trapping-region expression is

$$E(R_1) = -\frac{10^{-8}}{R_1} \left[\int_0^{a-w} \frac{dH'}{dt} R dR + \int_{a-w}^{R_1} \frac{dB_T}{dt} R dR \right], \quad (16)$$

where B_T is also obtained from (5), but using the plus (lower) sign.

In the circular region at radii $R_1 > R_0$, extending into the negative shielding regime, there are three terms in the expression for electric field:

$$E(R_1) = -\frac{10^{-8}}{R_1} \left[\int_0^{a-w} \frac{dH'}{dt} R dR + \int_{a-w}^{R_0} \frac{dB_T}{dt} R dR + \int_{R_0}^{R_1} \frac{dB_S}{dt} R dR \right]. \quad (17)$$

Again, H' is the field in the volume surrounded by the tube, given here by (4); and B_T and B_S are the induction in trapping and negative shielding layers, obtained from (10) and (8), respectively. At radii $R_1 < R_0$, extending only into the trapping layer, (17) reduces to

$$E(R_1) = -\frac{10^{-8}}{R_1} \left[\int_0^{a-w} \frac{dH'}{dt} R dR + \int_{a-w}^{R_1} \frac{dB_T}{dt} R dR \right]. \quad (18)$$

In all cases the integrations are of elementary functions.

Joule Power Density

If we now compute the Joule power density⁶⁻⁸

$$p_J = EJ, \quad (19)$$

we obtain a comprehensive picture of the radial distribution of this dissipation in the several regimes at various applied fields.⁹ For concreteness, we shall summarize the results of computations of B , J , E , and p_J for our unannealed $\text{Nb}_{0.75}\text{Zr}_{0.25}$ tubular sample No. 123, of 4 mm outside radius and 1.5 mm wall, for which $\alpha_c = 1.2 \times 10^8$ GA/cm² and $B_0 = 2.1$ kG.

⁶ P. W. Anderson and Y. B. Kim, Rev. Mod. Phys. 36, 39 (1964).

⁷ Y. B. Kim, C. F. Hempstead, and A. R. Strnad, Phys. Rev. 139, A1163 (1965).

⁸ Y. B. Kim, Phys. Today 17, No. 9, 21 (1964).

⁹ C. R. Wischmeyer, Phys. Letters 20, 578 (1966).

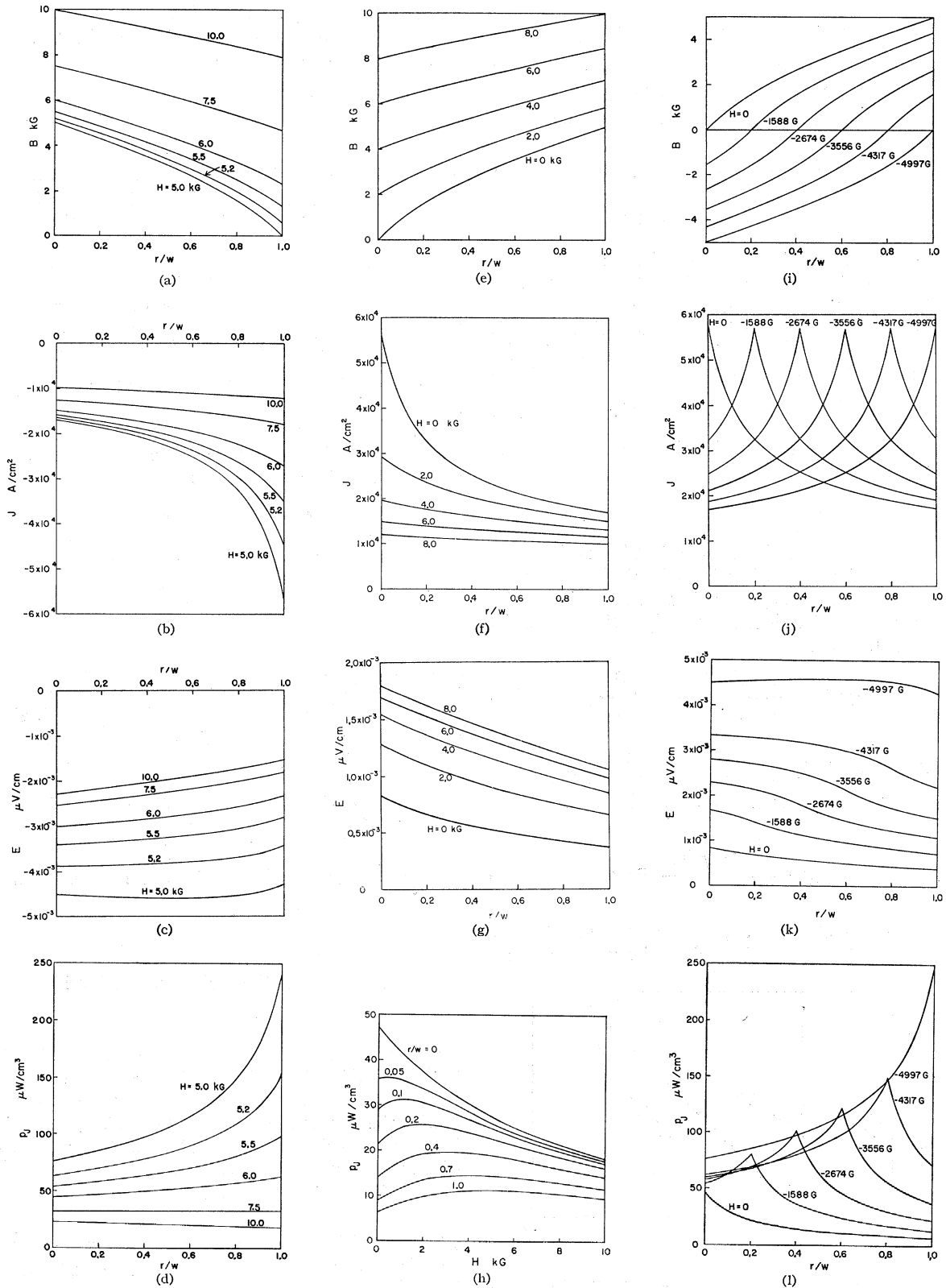
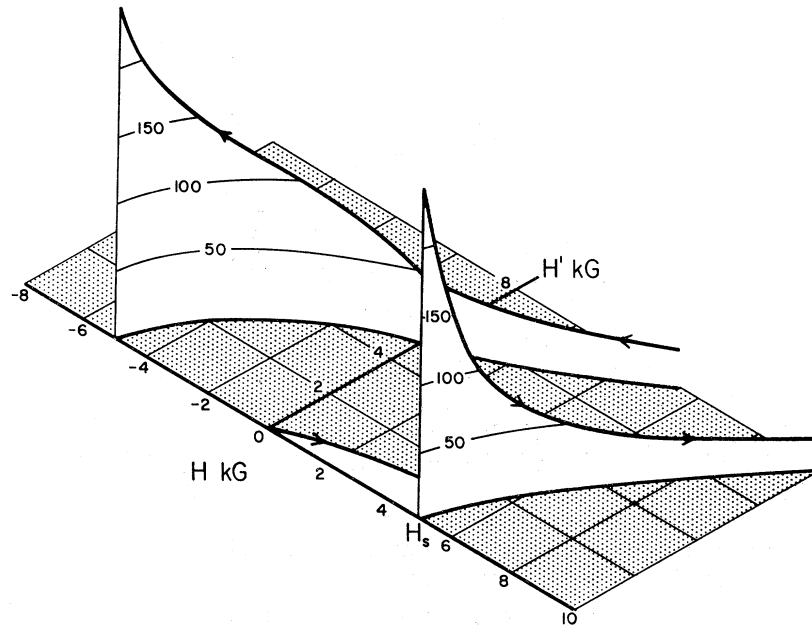


FIG. 3. Induction B , current density J , electric field intensity E , and Joulean power density p_J are plotted versus the ratio of radial depth to wall thickness. Corresponding curves for the shielding, trapping, and circular regions are shown from left to right. $H_s = 4997$ G.

FIG. 4. Greatest values of Joulean power density p_J in $\mu\text{W}/\text{cm}^3$ are plotted vertically along the critical state paths for a sample cooled in zero field. The sharp rise in p_J upon entering the shielding region at $H=H_s$ results when wall penetration is complete and H' starts to rise.



We shall examine the variations in B , J , E , and p_J along the critical-state $H-H'$ path, shown in Fig. 2, for a sample cooled in zero field. In all instances, the rate of change of applied field will be considered to be 1 G per second. Electric field E , induced by changing H , and consequently p_J , are proportional to dH/dt .

Increasing H positively causes a progressive penetration of a parabolic spatial distribution of magnetic field, decreasing from H at the outer surface of the tube to zero. For convenience, we let H_s represent the largest applied field at which the tube is capable of complete magnetic shielding, i.e., of maintaining $H'=0$. For $H < H_s$, there remains an undisturbed layer of superconductor ($B=0$) next to the inner surface of the tube wall. Although very large current densities are attained where the induction is small, the values of E tend rapidly toward zero beneath the outer surface. This leads to very modest values of p_J , which decrease to zero with depth r . Throughout the initial penetration range the greatest values of E and of p_J are at the outer surface of the tube.

As H exceeds H_s , the sample enters the shielding region. The shielding effect of the superconducting tube is no longer sufficient to maintain H' at zero. Flux creeps through the tube wall, and the sample is essentially in a critical state, i.e., as described by Kim *et al.*^{1,4} The lowest values of induction, and consequently the highest current densities, are at the inner surface of the wall. E tends to decrease with radial depth and with increasing H . Consequently a wide variation of p_J results, the greatest values occurring at the inner surface of the wall for $H=H_s$. (See Fig. 3.)

Reducing H , first along a non-critical-state path (H' remains constant), we then establish the trapping regime, in which the lowest values of induction, and

consequently the highest values of current density, are always at the outer surface. Again E decreases with radial depth and also decreases with decreasing H . Consequently, the greatest p_J values, though significantly smaller than in the shielding region, are now found on the outer surface of the tube and increase with decreasing H .

As H reaches zero and becomes negative, the sample enters the circular region. An outer layer now contains fluxoids of the negative applied field, while an inner layer retains fluxoids of the trapped field. At the interface adjacent fluxoids are oppositely directed. We visualize here another dissipative process, flux annihilation, which we shall discuss under a separate heading.

At a given H in the circular region, the variation of E across the tube wall is small; but E is roughly proportional to the magnitude of applied H . Consequently, the peaks of p_J coincide with those of J , which occur at the zeroes of induction B . The largest of these peaks occurs deep in the circular region, at the transition from circular to (negative) shielding region.

Figure 4 summarizes the field dependence of Joulean heating. The greatest values of p_J (regardless of the radii at which they occur) are plotted vertically for the corresponding points (H, H') . The sharp rise in p_J at $H=H_s$ marks the transition from the initial penetration range to the shielding region. Note that this same p_J is attained in the circular region as H' reaches zero. These values of p_J , which are averages in the sense that they are based upon assumed homogeneity of the sample, can by no means account for more than a miniscule temperature rise (typically tens of millidegrees at $dH/dt = 1 \text{ G/sec}$).

IV. FLUX ANNIHILATION

In the circular region, and not elsewhere, the outer layer of the sample contains fluxoids in the direction of the more recently applied field, while the inner layer retains trapped fluxoids of the former direction. In each regime, the fluxoids are driven toward the interface by Maxwell pressure. At the interface, we visualize each trapped fluxoid as coalescing with an opposing fluxoid produced by the applied field, both giving up their line energies in annihilation.^{10,11} (See Fig. 5.)

In developing the annihilation picture it is convenient to think of a radial corridor, perpendicular to the interface, and of width $\delta = (\varphi_0/B_{c1})^{1/2}$ cm, which is the line spacing of the Abrikosov flux structure at the lower critical field. By Faraday's law, the average radial velocity of the fluxoids will be $v = 10^8 E/B_{c1}$ cm/sec (E in V/cm, B in G).

Now, as H increases in the new (negative) direction, the interface itself moves slowly across the tube wall from the outside inwards at a velocity

$$dr_0/dt = 2.5(\pi\alpha_c)^{-1}(H - B_0)dH/dt, \quad (20)$$

which we obtain by differentiating (7). Typically the interface velocity is one or two orders of magnitude less than the fluxoid velocity at the interface.

Hence, an annihilation is expected to occur, on the average, every $\tau \approx \delta/v$ seconds in a corridor of width δ . Each fluxoid yields energy¹² $\epsilon = 10^{-7} \varphi_0 H_{c1}/4\pi$ J/cm of line length, or 2ϵ per event.

It is now possible to estimate an annihilation power density p_A by ascribing an energy 2ϵ to a time τ and a volume of radial extent $\tau dr_0/dt$ by δ measured circumferentially by 1 cm of axial length.

$$p_A = \frac{2\epsilon}{\tau^2 \delta dr_0/dt} = \frac{2 \times 10^8 \alpha_c E^2}{\delta (H - B_0) dH/dt}. \quad (21)$$

Again, for concreteness, we shall refer to our unannealed Nb_{0.75}Zr_{0.25} sample No. 123 at 4.2°K. For B_{c1} we use 200 G. p_A as a function of applied field is shown in Fig. 6. We estimate that power densities of this order,

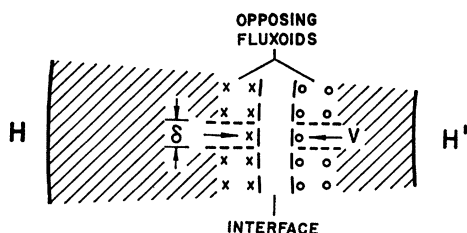


FIG. 5. Schematic representation of a portion of the tube cross section normal to the axis of the tube, showing a radial corridor of width δ . Fluxoids outside the interface would be expected to have a velocity somewhat greater than v , since in addition to sustaining the annihilation process, they must also advance the flux front.

¹⁰ C. R. Wischmeyer, Phys. Letters 18, 100 (1965).

¹¹ J. E. Evetts, A. M. Campbell, and D. Dew-Hughes, Phil. Mag. 10, 339 (1964).

¹² P. G. de Gennes and J. Matricon, Rev. Mod. Phys. 36, 45 (1964).

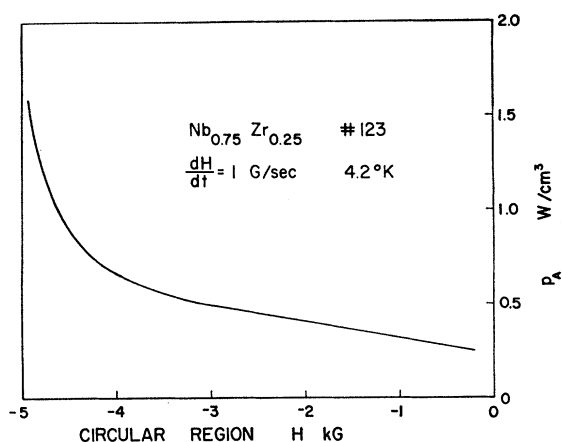


FIG. 6. Annihilation power density p_A increases with (negative) H . The interface in which annihilation is presumed to occur advances from the outside to the inside of the tube wall for the range of H shown.

which are seen to be four orders of magnitude greater than the accompanying Joulean values, are sufficient to raise the local temperature only about 3°K, not to T_c .

With $\delta = 3.2 \times 10^{-5}$ cm, the fluxoid velocity at the interface ranges from about 4×10^{-4} to 2×10^{-3} cm/sec. Corresponding dr_0/dt values are 1.5×10^{-5} to 4.6×10^{-5} cm/sec. This results in an average spacing (radially) of annihilation sites of $\tau dr_0/dt = 1.1 \times 10^{-6}$ cm to 0.8×10^{-6} cm.

V. EXPERIMENTAL OBSERVATIONS

Extensive experimental observations of flux creep⁴ activity and of flux jumps (catastrophic equilization of H' to H), to be reported in a subsequent paper, may be summarized as follows: The intensity of flux creep activity and of flux jumps has consistently been observed to rise from essentially zero to very great proportions at $H = H_S$ and then to decrease with increasing H . In the trapping region modest activity is observed to increase as H approaches zero. For many materials the incidence of flux-jumping seems always to be accompanied by severe flux-creep activity.

Activity in the circular region is qualitatively much more severe than anywhere else. In fact, at the lowest available dH/dt (< 1 G/sec), it was impossible to scan through more than a portion of the circular region without triggering a flux jump in our sample No. 123.

VI. CONCLUSIONS

The correlation between computed Joulean and annihilation power and observed flux-creep activity and flux jumps is definitive. Since the computed (average) values of dissipation are insufficient to raise the sample temperature to T_c , we conclude that they are significant as a trigger in providing thermal activation and that local variations of dissipation, for which there is ample evidence,⁵ are of crucial importance in the electromagnetic behavior of hard superconductors. In the circular

region, it is difficult to estimate the relative effectiveness of Joulean and annihilation dissipation as a trigger mechanism because of the completely different spatial distributions.

ACKNOWLEDGMENTS

The experimental work to which these computations relate was done at the Bell Telephone Laboratories,

Inc., Murray Hill, New Jersey, during a recent sabbatical. The author gratefully acknowledges his indebtedness to Dr. Y. B. Kim and his group there. For the impetus to undertake these detailed computations the author is indebted to Professor dr. M. J. Steenland, Technische Hogeschool te Eindhoven, and, for many stimulating discussions, to Dr. M. R. MacPhail, Rice University.

Superconducting- and Normal-State Thermal Conductivity of Impure Tin*

G. J. PEARSON,† C. W. ULBRICH,‡ J. E. GUETHS,‡ M. A. MITCHELL, AND C. A. REYNOLDS
Physics Department and Institute of Materials Science, University of Connecticut, Storrs, Connecticut

(Received 12 August 1965; revised manuscript received 20 June 1966)

Low-temperature measurements of the normal- and superconducting-state thermal conductivities were made on ten tin specimens, one of which was pure (99.996%) and nine of which were lightly doped (up to 1 at.%) with mercury, lead, or bismuth. The ratios K^s/K^n of the superconducting- to normal-state thermal conductivity are used to analyze the data. The normal-state thermal conductivity is assumed to consist of a fractionally small lattice component K_g^n consistent with the "universal-curve" formalism of Lindenfeld and Pennebaker, added to a much larger electronic component of the Wiedemann-Franz type. The superconducting lattice thermal conductivity K_g^s is assumed to be simply related to K_g^n in a manner roughly independent of impurity concentration. Proceeding in this manner, it is shown that the variation of K^s/K^n with changing electronic mean free path is consistent with a normal-state lattice conductivity having a temperature dependence similar to that observed by other investigators on other alloy systems. Furthermore, if one *quantitatively* adopts the "universal-curve" formalism, it is seen that the analysis yields a temperature-dependent ratio of lattice conductivities, K_g^s/K_g^n , which is consistent with the theory of Bardeen, Rickayzen, and Tewordt. The thermal conductivities of the pure and the three lowest impurity samples are mostly electronic, and thus it is possible to compare their K^s/K^n ratio with the theoretical K_e^s/K_e^n ratio of Kadanoff and Martin, calculated for an isotropic gap. The pure-sample data fit the theory with a value of $3.3k_B T_e$ for the superconducting energy gap. However, a value of $3.9k_B T_e$ is found for the gap for the three impure samples.

I. INTRODUCTION

DESCRIBED herein are the results of measurements taken at liquid-helium temperatures on each of one pure and nine impure samples of tin. Of primary interest is the thermal conductivity in the normal and superconducting states. Electrical resistivity and superconducting transition temperature determinations were also made to aid in the reduction and interpretation of the data.

We express the normal- and superconducting-state thermal conductivities as the sum of two terms, one electronic (e) and one lattice (g), viz:

$$\text{(normal state)} \quad K^n = K_e^n + K_g^n, \quad (1)$$

$$\text{(superconducting state)} \quad K^s = K_e^s + K_g^s. \quad (2)$$

* Supported by U. S. Air Force Office of Scientific Research Grant No. AF-AFOSR-474-64 and Office of Naval Research Contract No. Nonr 2967(00). Part of a thesis submitted by G. J. Pearson to the University of Connecticut in partial fulfillment of the requirements for the Ph.D. degree in Physics.

** Present address: Eastman Kodak, Rochester, New York.

† Present address: Clemson University, Clemson, South Carolina.

‡ Present address: Wisconsin State University, Oshkosh, Wisconsin.

Previous works on tin¹⁻⁵ have shown that in the temperature range of 1-4°K:

(a) For relatively pure samples (≤ 0.01 at. % impurity) the electronic thermal conductivity in the normal and superconducting states is the dominant mechanism. In particular, the normal-state thermal conductivity is adequately described by

$$1/K_e^n = \alpha T^2 + \beta/T, \quad (3)$$

where αT^2 is the ideal thermal resistivity, due to scattering of electrons by phonons, and β/T is the electron-impurity scattering term. β is approximately ρ_0/L_0 , where ρ_0 is the residual electrical resistivity and L_0 is the theoretical Lorenz number.

(b) At about 1 at. % impurity concentration, the β/T term in Eq. (3) has become large and also the lattice conductivity becomes a detectable portion of the total, of the order of several percent at 4°K.

¹ A. M. Guénault, Proc. Roy. Soc. (London) **A262**, 420 (1961).

² J. K. Hulm, Proc. Roy. Soc. (London) **A204**, 98 (1950).

³ M. Garfinkel and P. Lindenfeld, Phys. Rev. **110**, 883 (1958).

⁴ S. J. Laredo, Proc. Roy. Soc. (London) **A229**, 473 (1955).

⁵ N. V. Zavaritskii, Zh. Eksperim. i Teor. Fiz. **39**, 1571 (1960) [English transl.: Soviet Phys.—JETP **12**, 1093 (1961)].